

50 MeV electron beams accelerated by a terawatt scalable kHz laser

C. M. Lazzarini^{1,2**}, G. M. Grittani^{1°}, P. Valenta¹, I. Zymak¹, R. Antipenkov¹, U. Chaulagain¹, L. V. N. Goncalves¹, A. Grenfell¹, M. Lamac^{1,3}, S. Lorenz^{1,2}, M. Nevrkla^{1,2}, V. Sobr¹, A. Spacek^{1,2}, W. Szuba¹, P. Bakule¹, G. Korn¹ and S. V. Bulanov^{1,4}

¹ELI Beamlines Facility, The Extreme Light Infrastructure ERIC, Dolni Brezany, 25241, Czech Republic.

²Czech Technical University in Prague, FNSPE, Prague, 11519, Czech Republic.

³Faculty of Mathematics and Physics, Charles University, Prague, 12116, Czech Republic.

⁴National Institutes for Quantum Science and Technology KPSI-QST, Umemidai, 8-1-7, 619-0215 Kizugawa-shi, Kyoto, Japan.

We show the laser-driven acceleration of unprecedented, collimated (2 mrad) and quasi-monoenergetic ($\Delta E/E = 25\%$) electron beams with energy up to 50 MeV at 1 kHz repetition rate. The laser driver is a multi-cycle (15 fs) 1 kHz OPCPA system, operating at 26 mJ (1.7 TW). The scalability of the driver laser technology and the electron beams reported in this work pave the way towards developing high brilliance X-ray sources for medical imaging, innovative devices for brain cancer treatment and represent a step forward to the realization of a kHz GeV electron beamline.

I. INTRODUCTION

Electron accelerators are a cornerstone technology of modern society. They are used in their variations daily as strategic tools at the disposal of the healthcare system for medical imaging and cancer treatment. For example, medical linear accelerators already use electron beams up to 20 MeV for cancer radiotherapy [1]. Radio-frequency acceleration is the backbone of the technology driving these machines and it is nowadays, after its first demonstration in 1928 [2], generally acknowledged as an extremely reliable technology. Radio-frequency acceleration technology has nevertheless a fundamental limitation in their maximum achievable accelerating gradient to 100 MV/m that puts a constraint in terms of the size and, as a consequence, the cost. This inhibits the realization of compact accelerators as a source for free electron lasers, Thomson scattering x-ray sources, and high energy electron accelerators for radiotherapy. As of today, the only proven technology with the potential to overcome these limitations is laser-plasma acceleration [3], which can withstand accelerating gradients exceeding 100 MV/mm [4]. Its potential has in recent years motivated an extensive effort by numerous groups worldwide, leading to remarkable achievements, ranging from the demonstration of the first GeV laser-driven electron beams [5-7], to the acceleration of multi-GeV electrons via plasma guiding [8-9] as well as to the demonstration of free electron lasing [10]. The desire to translate these exceptional results into working machines resulted in the demonstration of stable electron beam operation over more than 24 hours [11] and the acceleration of quasi-monoenergetic (QME) electron beams at 1 kHz repetition rate [12,13]. With the typical charge per pulse on the order of pC [14-16], the resulting average current of a kHz laser wakefield accelerator (LWFA) is on the order of

[°]These authors contributed equally to this work

* e-mail: CarloMaria.Lazzarini@eli-beams.eu

nA, which, provided the electron beam energy is higher than 40 MeV, would be enough to enable several medical applications [17-18]. These groundbreaking achievements have been obtained by exploiting nonlinearities through gas-filled hollow core fiber compression down to single cycle laser pulses in order to reach the relativistic intensity on target required to drive the wake wave in the plasma, where the injected electrons can be accelerated up to 15 MeV [13]. Despite producing very stable electron beams, this technique is limited by the maximum laser power available and by the maximum coupling efficiency into the hollow core fiber; these further limit the acceleration length in the plasma and thus the maximum electron energy attainable. Moreover, LWFA driven by single cycle lasers is also sensitive to carrier envelope phase effects [19,20], posing an additional limit on the attainable electron beam energy and quality.

In this paper we show for the first time the production of collimated (2 mrad divergence) quasi-monoenergetic ($\Delta E/E = 25\%$ FWHM) electron beams with energy up to 50 MeV with multi-cycle (15 fs) laser pulses at 1 kHz repetition rate, overcoming the requirement of single cycle compression, and proving the energy scalability of the technology. This breakthrough has been achieved by ELI Beamlines' in-house development of the L1-Allegra multi- TW 1 kHz laser [21], based on optical parametric chirped pulse amplification technology (OPCPA). This laser key features for LWFA are its multi-stage power scalable design (final output expected > 100 mJ), the absence of nanosecond contrast being pumped by 3 ps Yb:YAG thin-disk lasers and its power and pointing stability (few % level) over many hours of continuous operation.

II. EXPERIMENT

The L1- Allegra laser was running six amplification stages (as shown in Fig.1a) achieving a pulse energy of 26 mJ, measured inside the interaction chamber. Optimal compression of the output pulses is achieved through a combination of chirped mirrors and initial stretching by a programmable acousto-optic modulator (Dazzler). Before the interaction chamber, the laser pulses were characterized both by measuring their near-field profile (Fig. 1b), having an elliptical shape, and by their time and spectrum characterization performed by a second harmonic generation frequency-resolved optical gating (SHG FROG) device, resulting in a pulse duration of 15 fs FWHM (Fig. 1c). The laser pulses were focused by a 76.2 mm focal length off-axis parabola down to a measured focal spot (Fig. 1d) with FWHM of 4.2 μm and 3.1 μm along the horizontal and vertical axes, respectively. This corresponds to an effective waist radius $w_0 = 3.1 \pm 0.3 \mu\text{m}$ and to a Rayleigh range $z_R = 37 \mu\text{m}$. Considering a central wavelength $\lambda_{laser} = 820$ nm, the resulting on-target peak intensity was $I_{peak} = 5.8 \times 10^{18} \text{ W/cm}^2$ (corresponding to a normalized vector potential $a_0 = 1.7$). The laser power available on target was $P_{laser} = 1.7$ TW, which, by considering the optimal electron density for this work of $n_e = 5.7 \times 10^{19} \text{ cm}^{-3}$, was well above the self-focusing threshold $P_{SF} = 0.52$ TW. This allows for self-guiding inside the plasma, as visible in the Thomson scattering diagnostic (Fig. 1e). The laser pulse was focused in the first half of the in-house designed and characterized [22,23] 300 μm diameter flat-top gas-jet, 150 μm above the nozzle exhaust (Fig. 1f). The gas target position has been optimized in three dimensions with accuracy at the level of the plasma wavelength $\lambda_{plasma} = 4.5 \mu\text{m}$, leading to the optimal focusing position inside the plasma profile.

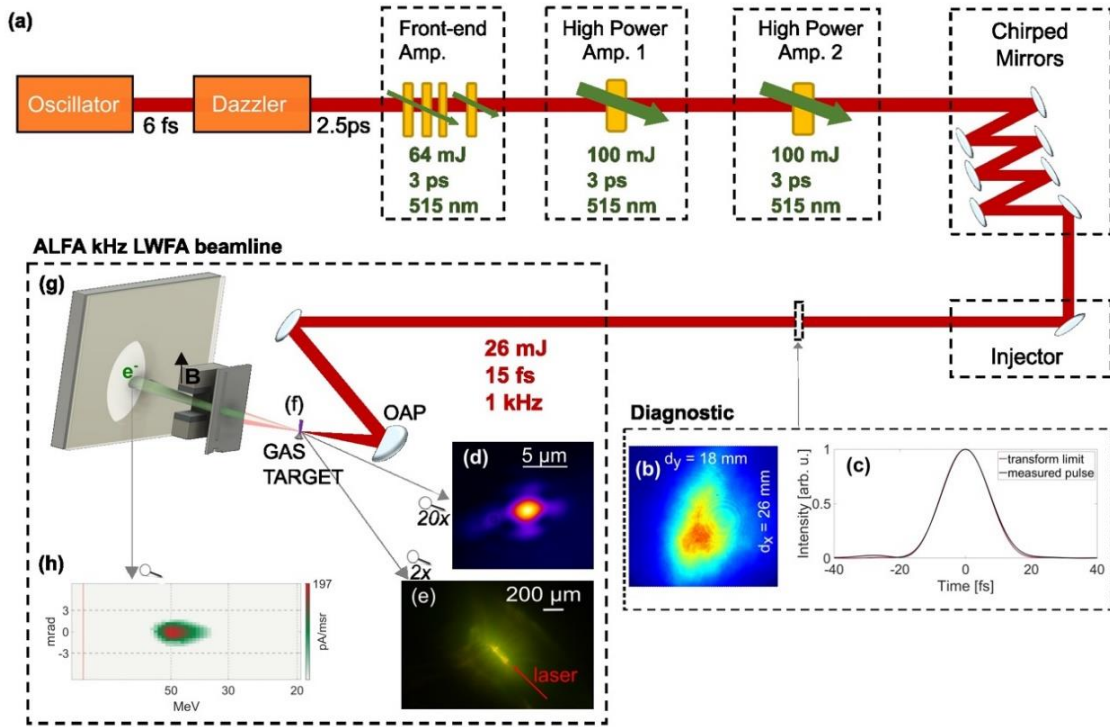


FIG. 1. (Color online). Simplified scheme of the experimental setup. (a) L1-Allegro laser system as used in this work, based on OPCPA stages and chirped mirror compressor. The pump sources (in green) are Yb:YAG thin-disk lasers. (b) The laser pulse near-field (NF) profile measured after the injector with Gaussian-fit diameters, giving an eccentricity $\varepsilon \approx 0.8$. (c) The pulse time duration measured by FROG device compared to the transform-limited value (in red). (d) Focal spot measured with a 20x apochromatic microscope objective. (e) High-magnification achromatic Thomson scattering spectrally filtered diagnostics. (f) Supersonic gas-jet target. (g) Electron spectrometer. (h) Electron beam trace on the Lanex.

The repeatability and stability of the acceleration process was assured by the laser contrast higher than 10^{10} at the ps-level (measured by the Sequoia cross-correlator), and basically not-present at the ns-scale thanks to the few ps pump lasers, and by the laser pointing stability (rms averaged horizontal and vertical) on target of $3.6 \pm 0.3 \mu\text{rad}$. The accelerated electron beams were characterized by a calibrated electron spectrometer (Fig. 1g) consisting of a motorized 5-mm collimator aluminum slit, a motorized 39 mm long 0.1 T permanent magnetic dipole, and a LANEX Fast Back scintillator screen captured by using a 12-bit CMOS global shutter camera (Fig. 1h).

The limited energy available from kHz laser systems requires a near-critical plasma density in order to enable relativistic self-focusing [13]. This in turn shortens the plasma wavelength to a few microns and ultimately results in the need of comparable resolution in the laser-plasma interaction diagnostics [28]. The laser-plasma interaction was optimized first at a reduced laser power of 0.8 TW, by carefully tuning the focus position inside the gas target profile monitored with a 5x magnification optical side-view and a 2x achromatic Thomson scattering spectrally filtered top-view diagnostics, both with a resolution smaller than λ_{plasma} .

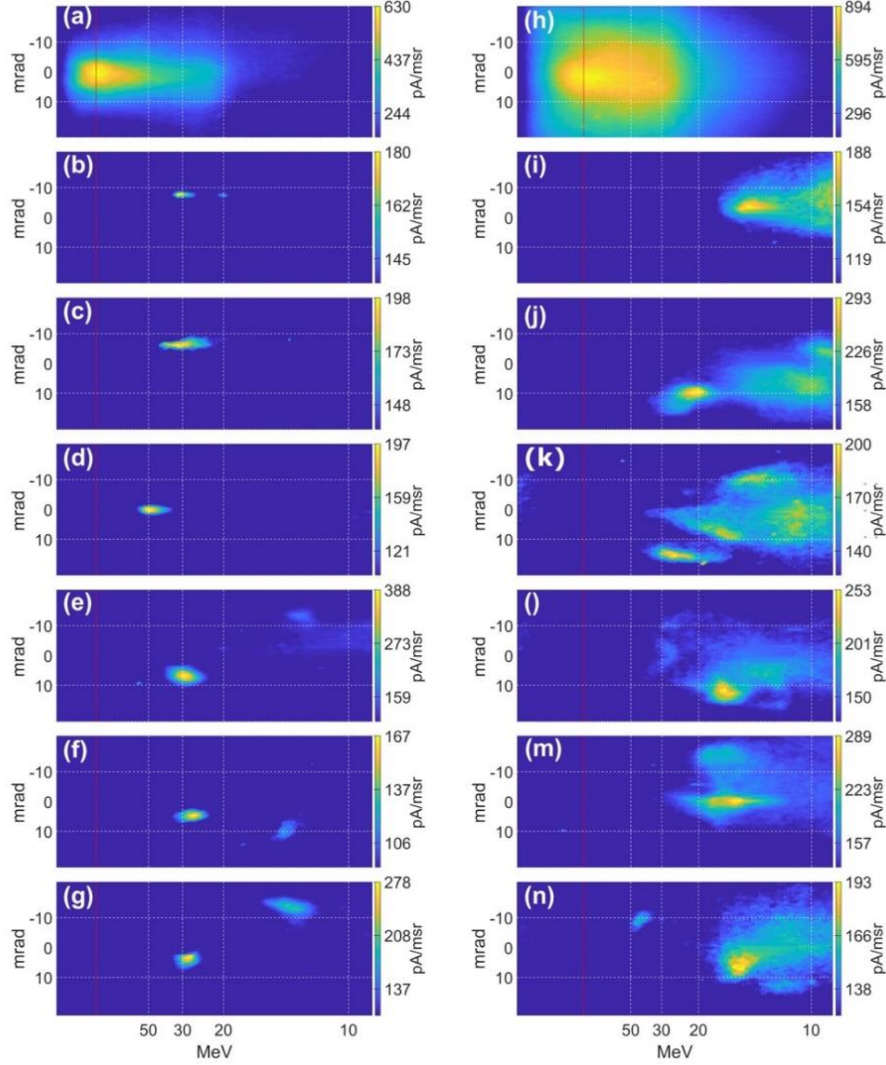


FIG. 2. (Color online). Transition to high-energy quasi-monoenergetic beams. (a) Reference electron trace on Lanex without magnetic field for the Nitrogen-Helium mixture target operating at a plasma density $n_e/n_{cr} = 0.034$. (b-g) Selected spectra with magnetic field on, showing monoenergetic characteristics. In (d) is shown the 50 MeV energy spectrum. (h) Electron trace with magnetic field off for the higher density case of $n_e/n_{cr} = 0.038$. (i-n) Selected spectra with magnetic field on. Each trace on the spectrometer is integrated over 10 consecutive laser pulses and has the background noise filtered out. For each case, the aperture slit is centered at the high-energy pointing position (red line) that represents the infinite-energy axis along the optical axis.

The gas pressure has been then tuned by an electronic valve in order to achieve simultaneously relativistic self-focusing and electron injection in the plasma wave. The laser pulses have been delivered on target at a 1 kHz repetition rate for the whole duration of the experiment, in order to reach thermal equilibrium in all the system components. The gas jet opening time, synchronized with the arrival of the driving pulse by a trigger, was set as either pulsed or continuous, depending on the regime of operation. In fact, it must be noted that the radiation level achieved by a kHz LWFA machine is well above the values typical for laser facilities. The possibility of running

continuous gas flow was enabled by a double differential pumping system, on target and before the compressor, which kept unaffected the laser-driven acceleration process throughout several hours of continuous operation. After observing quasi-monoenergetic beams with 0.8 TW, we gradually increased the laser energy up to 26 mJ (1.7 TW), iteratively optimizing the gas density and the focusing position inside the target density profile. In addition, the second order spectral phase has been optimized using an acousto-optic programmable dispersive filter (Dazzler in FIG. 1a) to compensate for the plasma medium dispersion and to extend the acceleration.

The most energetic and collimated electron beams have been obtained by firing the laser on a gas mixture of Helium (98%) and Nitrogen (2%), which allowed acceleration at an electron plasma density as low as $n_e = 5.7 \times 10^{19} \text{ cm}^{-3}$. This corresponds to a fraction of the plasma critical density $n_e/n_{cr} = 0.034$. In this configuration, record-high energy electron beams have been obtained, with energy up to 50 MeV (FIG. 2d). The electron energy is in a good agreement with the maximum energy gain expected in the quasi-linear case when limited by the dephasing length ($L_{deph} \approx 46 \text{ } \mu\text{m}$), i.e. $\Delta E_{GAIN} \sim L_{deph} \approx 48 \text{ MeV}$. By averaging over thousands of shots (a sample of which is shown in Fig. 2b-g) we observed an average energy of $32 \pm 5 \text{ MeV}$ (std), with an average energy spread of 8 MeV (25%, FWHM), and a beam divergence of $2.1 \pm 0.8 \text{ mrad}$ (FWHM). The LWFA process in this new space of parameters presents new challenges. In fact, despite obtaining very stable electron beams in the optimal configuration, small changes in any parameter can significantly affect the acceleration process. For example, a small change in the plasma density from $n_e/n_{cr} = 0.034$ to 0.038 (13%) results in a significant reduction of the beam energy and in the loss of the quasi-monoenergetic feature (FIG. 2i-n).

III. SIMULATIONS AND DISCUSSION

We investigated the electron acceleration for the experimental laser and plasma parameters also with three-dimensional (3D) particle-in-cell (PIC) simulations using the EPOCH [29] code. Here the driver pulse propagates in a pre-ionized plasma with an initial electron density profile obtained from a hydrodynamic simulation of the gas jet. The plasma is cold and collisionless, represented with electron quasi-particles moving on a static neutralizing background. The simulations utilize the technique of moving window with dimensions of $70 \lambda_0 \times 80 \lambda_0 \times 100 \lambda_0$. The underlying Cartesian grid is uniform with the resolution of 20 and 10 cells per λ_0 along the driver propagation direction and the transverse directions, respectively. The simulations were evolved over the time interval of 2.2 ps.

In the $n_e/n_{cr} = 0.034$ case, the driver pulse self-focuses in plasma and attains its peak normalized amplitude $a = 2.59$. Its spot sizes in plasma are 2.2 μm and 2.0 μm (FWHM) along the horizontal and vertical directions, respectively. The electron self-injection occurs in the vicinity of focus at several periods of the wake wave behind the driver except the first one (FIG. 3a). A second self-injection occurs when the driver enters the region of the electron density down-ramp, corresponding to the mechanism described in Ref. [30]. As a result, two distinct electron populations can be identified in the energy spectrum (FIG. 3b top). The electrons with energies in the ranges 5-15 MeV and 20-25 MeV originate from the second and first injection processes, respectively. The electrons originating from the first injection process acquire additional energy boost of 5 MeV in the rear part of the gas target.

At this time, most of the electrons in the beam appear at the top of the separatrix branch enclosing the trajectories of trapped electrons in phase space. Normally, the electrons would enter a decelerating phase of the wakefield. However, due to the decreasing electron density, the wakefield structure elongates, so that the electrons find themselves again in the accelerating phase for a short time, similarly as in the regime of dephasing-less

acceleration with tapered targets [34]. The electron energy spectrum at the end of the simulation contains two quasi-monoenergetic electron beams. The cut-off energies of both electron beams are 16.6 MeV and 27.4 MeV, whereas the energy spread of the higher energy beam is 1.9 MeV in FWHM (i.e., 8%). The charge and the FWHM divergence of electrons with kinetic energy $E_k \geq 20$ MeV are 1.7 pC and 19.4 mrad, respectively. By slightly reducing the density ($n_e/n_{cr} = 0.03$), the self-injection is suppressed resulting in a negligible amount of electrons being accelerated, in agreement with the experimental measurement.

In the opposite case, corresponding to a density increase to $n_e/n_{cr} = 0.038$, the driver pulse attains peak amplitude $a = 2.74$. Its radial profile becomes circular at focus with the spot size of 2.0 μm in FWHM. This case is characterized by fast driver energy depletion, which manifests itself in the carrier frequency downshift and slowing down of the pulse front [34]. After passing the focus, the driver splits into two distinct pulses, each consisting of only a few-cycles and propagating at a different velocity. Due to the short duration of both pulses and relatively dense plasma, the rapid evolution of their carrier-envelope phases causes oscillations of the wake wave cavities in the driver polarization direction as well as their longitudinal modulations, strongly affecting the parameters of self-injected electrons. Furthermore, the electrons injected into the first period of the wake wave interact with the rear part of the driver pulse. The resulting electron energy spectrum has thermal, relatively flat profile (FIG. 3b bottom). The cut-off energy of electrons is 33 MeV. The charge and the FWHM divergence of electrons with $E_k \geq 20$ MeV are 1.33 pC and 107.8 mrad, respectively.

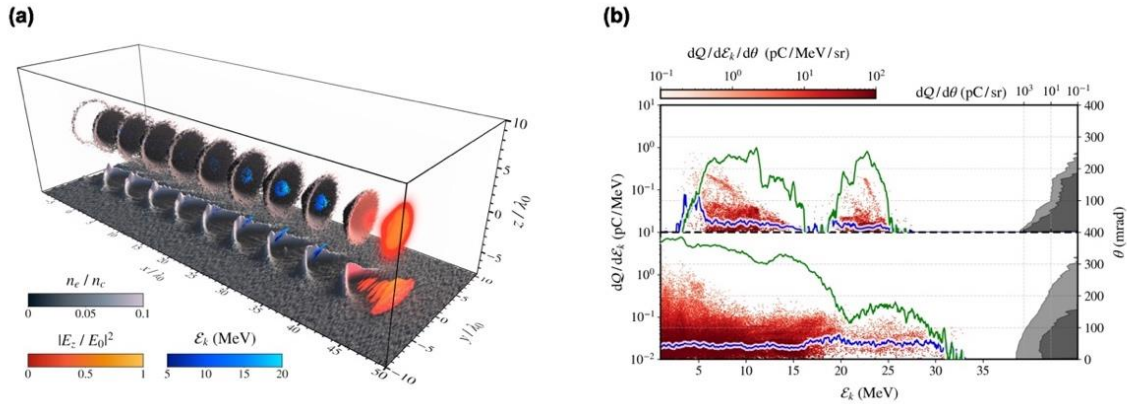


FIG. 3. (Color online). PIC simulations results. (a) 3D visualization of the data from the $n_e/n_{cr} = 0.034$ case simulation showing the electron number density (black to white colormap), driver pulse intensity (red to yellow colormap), and the injected electrons with $E_k \geq 5$ MeV (dark to light blue colormap). (b) Electron energy spectrum dQ/dE_k (green line), average electron propagation angle θ (blue line), charge density of electrons with respect to the propagation angle $dQ/d\theta$ including electrons with $E_k \geq 1$ MeV (light gray) and $E_k \geq 20$ MeV (dark gray), and charge density of electrons with respect to the kinetic energy and propagation angle $dQ/dE_k/d\theta$ (white to red colormap) for (upper) $n_e/n_{cr} = 0.034$ and (lower) $n_e/n_{cr} = 0.038$ cases.

By increasing the plasma density even more, i.e., operating at $n_e/n_{cr} = 0.042$, the simulations indicate that the regime of laser-plasma interaction does not change substantially. Even though a larger fraction of electrons gets trapped resulting in a higher beam charge, the pulse depletion is stronger, which reduces both the acceleration length and the maximum reachable electron energy.

The PIC simulations clearly reproduce the transition from the quasi-monoenergetic to the broadband electron energy spectra with the increase of the plasma density over the same values observed experimentally (FIG. 2), with good agreement on the electron beam distribution.

IV. OPTIMIZATION FOR APPLICATIONS

Since the medical applications mentioned above rely on high current electron beams at relevant energies (> 20 MeV), we have optimized our LWFA source in two main modes of operation, that were freely entitled the high energy mode and the high power mode. The first one, described above and shown in Fig. 2a-g, had the beam energy and collimation maximized by tweaking the laser-plasma interaction at the lowest possible plasma density (given the available laser power). In the high power mode, the approach was to optimize the electron beam power by working at a slightly higher plasma density, sacrificing a bit the average peak energy and collimation. The fact that higher beam charge can be obtained at lower electron beam energies is likewise observed in other experiments [8]. The key parameters of the two modes of operation are summarized in Table I. With our current setup in the *high power mode*, we estimated a dose rate exceeding 1 Gy/s for beam sizes of few mm, that could lead to the first demonstration of laser-driven stereotactic radiosurgery in a similar setup to the one done at Lund [18], showing that approximately 600 shots were necessary to deposit 1 Gy in 1 cm³ target volume.

<i>Feature</i>	<i>High energy mode</i>	<i>High power mode</i>
Energy	32 ± 5 MeV	22 ± 2 MeV
Energy Spread (FWHM)	8 MeV (25%)	15 MeV (68%)
Current	12 ± 6 pA	276 ± 28 pA
Divergence (FWHM)	2.1 ± 0.8 mrad	7.8 ± 1.2 mrad
Pointing (std)	6.9 mrad	4.2 mrad
Electron Beam Power Output	0.4 mW	6 mW

TABLE I. Electron beam averaged parameters for the *high energy* and the *high power mode*.

V. CONCLUSION

In conclusion, the quasi-monoenergetic electron beams we generated at 1 kHz repetition rate with an unprecedented energy up to 50 MeV pave the way towards establishing LWFA technology as an innovative tool for treatment of small tumors (e.g., brain metastasis) and for the generation of high flux mono-energetic x-ray beams in the medical imaging range (20-50 keV). The latter can represent an unique source for x-ray fluorescent imaging (XFI), Phase Contrast Imaging (PCI) and micro-beam radiotherapy. Finally, we want to highlight that the shown all-reflection LWFA setup based on OPCPA technology is fully scalable in laser power, so this could allow reaching GeV-class electron beams at 1 kHz. Further work in all these directions is ongoing with the final goal to produce a stable and reliable high-energy, high-flux electron beamline for innovative user experiments.

ACKNOWLEDGEMENTS

We thank H. Milchberg for the very fruitful discussions. We acknowledge the helpful feedback on the manuscript from E. Chacon Golcher and J. Limpouch. We also acknowledge M. Favetta, G. Tasselli, F.I.M. Fucilli and M. Piombino for the availability of the medical linear accelerator used to calibrate the electron spectrometer. This work was supported by the projects "Advanced research using high-intensity photons and particles" (CZ.02.1.01/0.0/0.0/16_019/0000789) and "High field initiative" (CZ.02.1.01/0.0/0.0/15_003/0000449) from the European Regional Development Fund and by the project e-INFRA CZ (ID:90140) from the Ministry of Education, Youth and Sports of the Czech Republic.

AUTHORS CONTRIBUTIONS

R.A., P.B., A.G., V.S., A.S. and W.S. are the L1-Allegro laser team. G.K. had the idea for this experiment. The ALFA LWFA beamline was conceived and designed by C.M.L. and G.M.G. and its testing and full integration to the laser system was performed by C.M.L., G.M.G., I.Z., S.L., M.N., L.V.N.G., R.A., P.B. and V.S. The optical layout of the accelerator was designed and installed by C.M.L. with the help of M.N., L.V.N.G., G.M.G. and I.Z. The modelling of the plasma interaction and acceleration has been studied by P.V. and S.V.B. The experiment was coordinated by C.M.L. and G.M.G. All the data analysis has been performed by I.Z., C.M.L. and G.M.G. Written and prepared by C.M.L., G.M.G., I.Z., A.S., P.V., G.K. and S.V.B.

REFERENCES

1. D.E. Citrin, *Recent Developments in Radiotherapy*, N. Eng. J. Med. 377, 1065-1075 (2017).
2. R. Wideroe, *Über ein neues Prinzip zur Herstellung hoher Spannungen*, Archiv für Elektrotechnik 21, 387–406 (1928).
3. T. Tajima and J.M. Dawson, *Laser Electron Accelerator*, Phys. Rev. Lett. 43, 267 (1979).
4. E. Esarey, C.B. Schroeder and W.P. Leemans, *Physics of laser-driven plasma-based electron accelerators*, Rev. Mod. Phys. 81, 1229 (2009).
5. S. P. D. Mangles, et al., *Monoenergetic beams of relativistic electrons from intense laser–plasma interactions*, Nature 431, 535 (2004).
6. C. G. R. Geddes, Cs. Toth, J. van Tilborg, E. Esarey, C.B. Schroeder, D. Bruhwiler, C. Nieter, J. Cary and W.P. Leemans, *High-quality electron beams from a laser wakefield accelerator using plasma-channel guiding*, Nature 431, 538 (2004).
7. J. Faure, Y. Glinec, A. Pukhov, S. Kiselev, S. Gordienko, E. Lefebvre, J.-P. Rousseau, F. Burgy and V. Malka, *A laser–plasma accelerator producing monoenergetic electron beams*, Nature 431, 541 (2004).
8. A.J. Gonsalves et al., *Petawatt Laser Guiding and Electron Beam Acceleration to 8 GeV in a Laser-Heated Capillary Discharge Waveguide*, Phys. Rev. Lett. 122, 084801 (2019).
9. B. Miao et al., *Multi-GeV electron bunches from an all-optical laser wakefield accelerator*, Phys. Rev. X 12, 031038 (2022).
10. W. Wang et al., *Free-electron lasing at 27 nanometres based on a laser wakefield accelerator*, Nature 595, 516–520 (2021).
11. A.R. Maier et al. *Decoding Sources of Energy Variability in a Laser-Plasma Accelerator*, Phys. Rev. X 10, 031039 (2020).
12. D. Guenot et al., *Relativistic electron beams driven by kHz single-cycle light pulses*, Nat. Phys. 11, 293 (2017).
13. F. Salehi, M. Le, L. Railing, M. Kolesik and H. Milchberg, *Laser-Accelerated Low-Divergence 15 MeV Quasi - monoenergetic Electron Bunches at 1 kHz*, Phys. Rev. X 11, 021055 (2021).
14. A.J. Goers, G.A. Hine, L. Feder, B. Miao, F. Salehi, J.K. Wahlstrand and H. Milchberg, *Multi-MeV Electron Acceleration by Subterawatt Laser Pulses*, Phys. Rev. Lett. 115, 194802 (2015).
15. D. Gustas, D. Guenot, A. Vernier, S. Dutt, F. Bohle, R. Lopez-Martens, A. Lifschitz and J. Faure, *High-charge relativistic electron bunches from a kHz Laser-Plasma Accelerator*, Phys. Rev. Accel. Beams 21, 013401 (2018).

16. F. Salehi, A.J. Goers, G.A. Hine, L. Feder, D. Kuk, B. Miao, D. Kuk, B. Miao, D. Woodbury, K.Y. Kim and H. Milchberg, *MeV electron acceleration at 1 kHz with <10mJ laser pulses*, Opt. Lett. 42, 215 (2017).
17. T. Brummer, A. Debus, R. Pausch, J. Osterhoff and F. Grüner, *Design study for a compact laser-driven source for medical x-ray fluorescence imaging*, Phys. Rev. Accel. Beams 23, 031601 (2020).
18. L. Svendsen, et al. *A focused very high energy electron beam for fractionated stereotactic radiotherapy*, Sci. Rep. 11, 5844 (2021).
19. P. Valenta, T. Zh. Esirkepov, J.K. Koga, A. Necas, G.M. Grittani, C.M. Lazzarini, O. Klimo, G. Korn and S.V. Bulanov, *Polarity reversal of wakefields driven by ultrashort pulse laser*, Phys. Rev. E 102, 053216 (2020).
20. J. Hujits, L. Rovige, I.A. Andriyash, A. Vernier, M. Ouille, J. Kaur, Z. Cheng, R. Lopez-Martens and J. Faure. *Waveform Control of Relativistic Electron Dynamics in Laser-Plasma Acceleration*, Phys. Rev. X 12, 011036 (2022).
21. Antipenkov, R. et al. *TW-class Allegra Laser System at ELI-Beamlines*, Proc. SPIE 11777, *High Power Lasers and Applications*, 11770E (2021). <https://doi.org/10.1117/12.2592432>.
22. S. Lorenz, G. Grittani, E. Chacon-Golcher, C.M. Lazzarini, J. Limpouch, F. Nawaz, M. Nevrkla, L. Vilanova and T. Levato, *Characterization of supersonic and subsonic gas targets for laser wakefield electron acceleration experiments*, Matter and Radiation at Extremes 4, 015401 (2019).
23. S. Lorenz, G.M. Grittani, L.V.N. Goncalves, C.M. Lazzarini, J. Limpouch, M. Nevrkla, S.V. Bulanov and G. Korn, *Tomographic reconstruction algorithms for structured gas density profiles of the targets for laser wakefield acceleration*, Meas. Sci. Technol. 31, 085205 (2020).
24. C. Ahdiba, et al. *New Capabilities of the FLUKA Multi-Purpose Code*, Front. Phys. 27, (2015). <https://doi.org/10.3389/fphy.2021.788253>.
25. G. Battistoni, et al. *Overview of the FLUKA code*, Ann Nucl. Energy 82, 10-18 (2015) <https://doi.org/10.1016/j.anucene.2014.11.007>
26. O. Chubar, P. Elleaume and J. Chavanne, *A three-dimensional magnetostatics computer code for insertion devices*, J. Sync. Rad. 5, 481-484 (1998). <https://doi.org/10.1107/S0909049597013502>.
27. D.A. Dahl, *SIMION for the personal computer in reflection*. Innt. J. Mass Spectrom. 200, 3-25 (2000). [https://doi.org/10.1016/S1387-3806\(00\)00305-5](https://doi.org/10.1016/S1387-3806(00)00305-5).
28. C.M. Lazzarini, L.V.N. Goncalves, G.M. Grittani, S. Lorenz, M. Nevrkla, P. Valenta, T. Levato, S.V. Bulanov and G. Korn, *Electron acceleration at ELI-Beamlines: Towards high-energy and high-repetition rate accelerators*, Int. J. Mod. Phys. A 34, 1943010 (2019).
29. T.D. Arber, et al. *Contemporary particle-in-cell approach to laser-plasma modelling*, Plasma Phys. Control. Fusion 57, 113001 (2015).
30. S.V. Bulanov, N.M. Naumova, F. Pegoraro and J.-I Sakai, *Particle Injection into the Acceleration Phase of the Wake Field behind the Laser Pulse*, Phys. Rev. E 58, 5257 (1998).
31. S. V. Bulanov, T. Zh. Esirkepov, Y. Hayashi, H. Kiriya, J. K. Koga, H. Kotaki, M. Mori and M. Kando, *On some theoretical problems of laser wake-field accelerators*, J. Plasma Phys. 82, 905820308 (2016).